Error Compensation for Low-Density Circular Gratings Based on Linear Image-Type Angular Displacement Measurements

Hai Yu ⓘ, Qiuhua Wan, Changhai Zhao ⓘ, Qingyang Han, and Zhiya Mu

Abstract—The image-type angular displacement measurement method based on linear image recognition has garnered attention because of its higher frequency response, strong fault tolerance, and high robustness. In the small-size image angular displacement measuring device, due to the limited pixel size, the circular grating cannot place more lines when realizing single-channel absolute coding recognition on a small diameter grating disk. This leads to larger errors in angular displacement measurement when the line density of the grating disk is low. To improve the measurement accuracy of small-scale displacement, the present work aimed to reduce this error by studying the error compensation method involving low-density grating disks. First, the mechanism of linear image-type angular displacement measurements is described, and a measurement algorithm based on linear scan images is proposed. Second, the measurement error model for low-density grating disks is established according to the proposed measurement algorithm. Third, a simplified error compensation algorithm based on a harmonic model is developed. Finally, simulations and experiments are performed to verify the performance of the proposed algorithm. Simulation results show that the developed harmonic compensation algorithm can effectively reduce the error caused by the low-density circular grating. When the proposed error compensation algorithm is applied to a grating disk with a 62 mm diameter and 2^N lines, the measurement accuracy is improved from 8.14" to 4.78". The proposed error compensation algorithm can significantly improve the accuracy of linear image-type angular displacement measurements involving low-density grating disks, and the results presented herein laid a foundation for improving the accuracy and engineering applicability of angular displacement measurement technology.

Index Terms—Error compensation, image-type displacement sensor, low-density grating disk.

I. INTRODUCTION

THE performance of digital displacement measurement technology directly affects the technical capabilities of the numerical control system [1], [2]. To date, the most commonly used displacement measurement strategies include optical grating measurements [3], [4], capacitive grating measurements [5], [6], and magnetic grating measurements [7], [8]. Among these approaches, the grating measurement method is used in a wide range of applications because of its high measurement accuracy and ease in realizing large-scale measurements. Most of the traditional grating displacement measurement methods employ Moiré fringe measurements, which must rely on high-density grating disks to achieve high resolution [9]. Additionally, the traditional approach requires cooperation between multiple coded channels to obtain absolute displacement measurements. Therefore, there are cumbersome steps such as an alignment period and a staggering phase during the assembly and adjustment processes. Additionally, once the relative position of the optical element changes, the preset signal relationship also changes, resulting in inaccurate measurements and even serious errors.

Image-type angular displacement measurement (I-ADM) technology represents a new photoelectric displacement measurement method [10], which uses image sensors for pattern recognition on a grating disk, and then performs displacement measurements according to a digital image processing algorithm [11], [12]. Owing to the high flexibility of the digital image processing algorithm, I-ADM technology demonstrates high robustness and fault tolerance [13]. By implementing subpixel image recognition, I-ADM technology can achieve high measurement resolution without relying on a high-density grating disk. Therefore, I-ADM technology is a good candidate for studying high-performance displacement measurement strategies.

Numerous scholars have launched research efforts investigating I-ADM. For example, Leviton [14] used an area scan image sensor to receive grating patterns engraved with reference lines and binary symbols, and the system's angular resolution reached 0.01". Additionally, in 2008, Sugiyam *et al.* [15] employed absolute displacement measurement technology with an area scan detector to achieve 14-b I-ADM resolution on a circular grating (diameter = 30 mm). Interestingly, Baji *et al.* [16] proposed a displacement measurement method based on color recognition, and ultimately achieved a measurement error of 1°. Although

some scholars have implemented I-ADM technology based on image sensors, challenges still remain, including the difficulty in enhancing the measurement frequency response from the area scan image sensor.

To improve the measurement frequency response, the use of linear scan image sensors to recognize the pattern of a grating disk has recently emerged as the main principle behind linear scan image-type angular displacement measurements (LI-ADM). Therefore, it is necessary to determine the suitable single-channel grating disks for LI-ADM. Previously, Kim *et al.* [17] used an M-sequence phase-shifting coding method to cooperate with a micro image detection system to realize 13-b coding recognition on a 41.72 mm diameter grating, and obtained an angle measurement accuracy of 0.044°. Mu *et al.* [18] used M-sequence pseudorandom code to recognize a 20-b pseudorandom sequence code. Yuan *et al.* [19] found that angular measurement accuracy of 1.9" could be achieved on a 79 mm diameter grating using a linear scan image sensor combined with M-sequence coding. Although these studies have generally met the needs of angular displacement measurements based on linear scan images, the research foundation regarding error compensation is still relatively limited in scope.

Our group previously proposed an error self-correction method based on dual image sensors [20]. The correction method for long period error using a single image sensor was also studied [21]. According to previous research, LI-ADM technology has great advantages in displacement measurement, but in the small-size measuring devices, the diameter of the circular grating used is relatively small. Due to the limited pixel size, when the absolute measurement of a single code channel is realized by an image sensor, the recognition of too dense lines cannot be realized. Too dense lines will make the spacing between lines very small, which leads to two problems: first, too dense markings are not conducive to coding recognition. Second, it is difficult to manufacture high-density code disks in industrial applications. Therefore, when the size of the circular grating is small, the number of lines will be reduced accordingly. Based on these, it was determined that a low line density on the grating disk in LI-ADM leads to errors when using a linear image sensor. Therefore, the present work involves the development of a measurement error compensation method for low-density grating disks in LI-ADM. First, the error model of a low-density grating disk is established, according to the LI-ADM mechanism. Then, a harmonic error compensation algorithm that is suitable for engineering applications is proposed. Finally, the proposed error compensation method is applied to an experimental device to verify the performance of the developed algorithm. Experiments indicate that the proposed error compensation method can effectively reduce the measurement error caused by a low-density grating disk. Therefore, the proposed method offers a theoretical foundation for improving the accuracy of LI-ADM.

The layout of this article is as follows. Section II describes the mechanism of LI-ADM, and describes the displacement measurement algorithm. Section III establishes the measurement error model involving a low-density grating disk, and proposes a harmonic error compensation method. Section IV discusses the
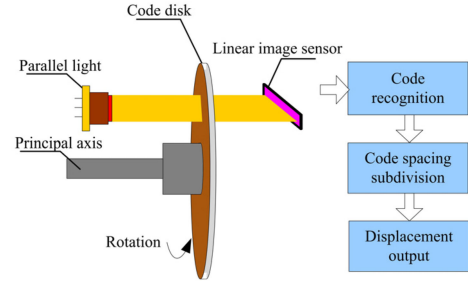

Fig. 1.   Schematic diagram of LI-ADM technology.

simulation verification, and Section V describes the experimental verification. Finally, Section VI concludes this article.

II. MECHANISM OF LI-ADM

A. Measuring Optical Path

LI-ADM technology is a flexible digital displacement measurement technique that uses a parallel light source to illuminate the grating disk and then projects the pattern on the disk onto the linear scan image sensor. The angle information of the current spindle rotation is transformed into the digital displacement measurement value via a digital image recognition algorithm. The measuring optical path is shown in Fig. 1.

The depiction in Fig. 1 includes the spindle, parallel light beam, grating disk, and linear scan image sensor. To measure the angular displacement, it is necessary to mark lines on the grating disk. During measurement, the parallel light source and linear scan image sensor are fixed, and the grating disk rotates coaxially with the main shaft. After the linear scan image sensor obtains the grating disk image, the processing circuit conducts operations, including code recognition and code spacing subdivision to obtain high-performance displacement measurements and output.

B. Displacement Measurement Algorithm

To perform LI-ADM, the image processing algorithm must achieve coding recognition and subdivision on the grating disk. Detailed studies have investigated the early stages of the coding recognition and decoding processes [22], [23]. Since the ultimate measurement accuracy of LI-ADM depends on the subdivision operation of the spacing between lines, only the subdivision operation is discussed herein.

Assuming that 2^N lines are evenly distributed on the grating disk [Fig. 2(a)], then during the linear scan image acquisition, the acquired image will contain at least two adjacent lines' patterns [Fig. 2(b)].

In Fig. 2(b), *a* and *b* represent two lines located on either side of the image center point in an acquired image. For computational convenience, the *x-o-y* coordinate system was established, with the midpoint of the image as the coordinate origin, the gray value as the *y*-axis, and the pixel positions as the *x*-axis. The centroid algorithm was used to calculate the centroids of line *a*
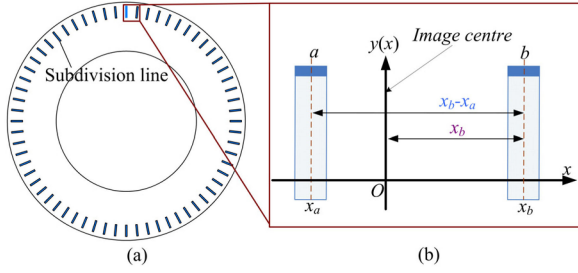
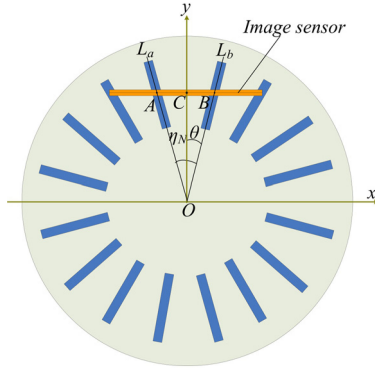Fig. 2.   Distribution of subdivision reference lines.

Fig. 3.   Actual physical position of 2^N lines.

and line b, expressed as x_a and x_b, respectively, using (1).

$$x_a(x_b) = \frac{\sum_{x \in a(b)} x \cdot y^2(x)}{\sum_{x \in a(b)} y^2(x)}. \qquad (1)$$

Then, according to the relationship between lines a and b in the coordinate system, the angular measurement operation can be calculated using (2).

$$S = 2^M \frac{x_a}{x_b - x_a} \qquad (2)$$

where 2^M represents the measurement multiple, which is the mapping value of the line spacing. The larger the 2^M value, the higher resolution of the displacement measurement. However, in practical application, subject to acquisition noise and other factors, the value of 2^M is generally less than 2^{16} when no denoising algorithm is used.

III. ERROR COMPENSATION OF LOW-DENSITY CIRCULAR GRATING

A. Error Model Establishment

Because the circular grating in practical applications has a given radian, the two adjacent lines have a corresponding angle between them. This leads to a certain measurement error in the algorithm presented in (2), and Fig. 3 shows the actual physical position of 2^N lines on the circular grating.

In Fig. 3, a polar coordinate system is established based on the center of the grating disk. The linear scan image sensor intersects with lines L_a and L_b at points A and B, respectively, and point C is

the center of the linear scan image sensor. The linear scan image sensor can only detect the pixel position information in the x-axis direction in such displacement measurements. Therefore, the positions of points A and B can be calculated using the centroid algorithm in (1). According to the relationship between ΔABO, the relationships in (3) and (4) can be established,

$$BC = \tan(\theta) \cdot OC \qquad (3)$$

$$BA = \tan(\theta) \cdot OC + \tan(\eta_N - \theta) \cdot OC \qquad (4)$$

where η_N is the angle between adjacent lines. Its polar coordinate form is expressed by (5).

$$\eta_N = \frac{2\pi}{2^N}. \qquad (5)$$

According to the algorithm in (2), the length of BC in the linear scan image corresponds to the value of x_b, and the length of BA corresponds to the value of x_b-x_a. Therefore, introducing the relationships $x_b = BC$ and x_b-$x_a = BA$ into (2) leads to (6).

$$S = \eta_N \cdot \frac{BC}{BA} = \eta_N \cdot \frac{\tan(\theta) \cdot OC}{\tan(\theta) \cdot OC + \tan(\eta_N - \theta) \cdot OC}. \qquad (6)$$

Therefore, when the linear scan image sensor is used for displacement measurements, the error can be calculated using the measurement error model of the low-density code disk shown in (7).

$$\mu = S - \theta = \left[\eta_N \cdot \frac{\tan(\theta)}{\tan(\theta) + \tan(\eta_N - \theta)} - \theta \right] \cdot \frac{180°}{\pi}. \qquad (7)$$

It can be seen, when $\theta = 0$, $\eta_N/2$, or η_N, the error μ will be zero. The range of (7) is proportional to the value of η_N, such that the greater the angle η_N, the greater the error value μ.

B. Error Compensation Algorithm

To achieve error compensation, the derived error value must be subtracted from the measured value. Because the error model in (7) is relatively more complicated, when this equation is used for error compensation, the algorithm implementation is also more complicated. Therefore, the error compensation model must be simplified.

To derive the changes in the error model, the error curves corresponding to circles with various numbers of lines ($2^N = 2^6$; $2^N = 2^7$; $2^N = 2^8$; $2^N = 2^9$) were plotted based on (7), as shown in Fig. 4. As the value of N decreased, the amplitude of the error curve gradually increased. When $N > 8$, the margin of error was close to 0", and this negligible error could be ignored.

The error model curve in Fig. 4 indicates that within the range of $0 \sim \eta_N$, the fluctuation of the error approximately follows a sine function. It is also clear that as the value of N decreases, the value of η_N and the frequency of the error curve also decrease. Based on the evaluated values of N, the change in the error frequency curve was always 2^N.

Therefore, when the number of lines is 2^N, a harmonic error component with a frequency of 2^N is generated. Thus, it is reasonable to assume that the harmonic component can be approximately expressed as $c_N \sin(2^N \cdot \theta)$, where c_N is the harmonic coefficient. Overall, the measurement error caused by
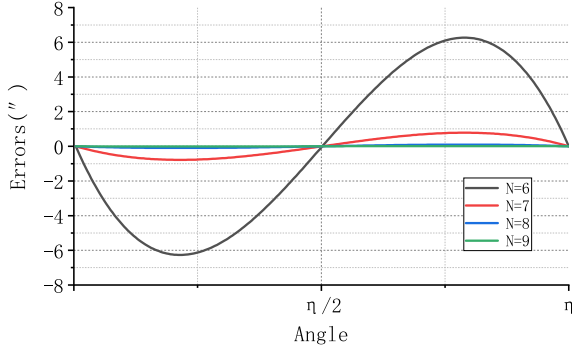
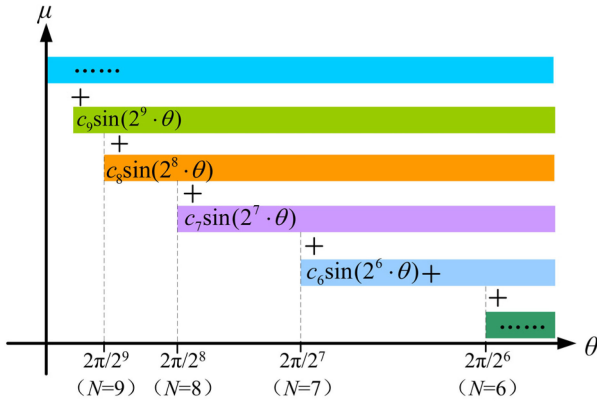Fig. 4. Error curve for circles with various numbers of lines.

Fig. 5. Relationships between harmonic components.

a low-density grating disk is the sum of the sine components of multiple frequencies, and the relationship between the sine components of each period is shown in Fig. 5.

For different values of N, the compositions of harmonic components are distinct (Fig. 5). The measurement error can therefore be approximately expressed as the sum of all harmonic errors with frequencies greater than 2^N, as shown in the harmonic error model of the low-density code disk:

$$\mu_N \approx \sum_{i=N}^{\infty} c_N \sin(2^N \cdot \theta) \approx \sum_{i=N}^{\infty} c_N \sin\left(2\pi \cdot \frac{\theta}{\eta_N}\right) \quad (8)$$

where, corresponding to different values of N, the value of η_N is also different.

Based on this, the angle measurement value after compensation can be calculated using (9), which represents the proposed error compensation algorithm for LI-ADM.

$$\theta' = S - \mu_N$$

$$\approx 2^M \frac{\theta}{\eta_N} - c_N \sin\left(2\pi \cdot \frac{\theta}{\eta_N}\right) - c_{N+1} \sin\left(2\pi \cdot \frac{\theta}{\eta_N/2}\right)$$

$$- c_{N+2} \sin\left(2\pi \cdot \frac{\theta}{\eta_N/2^2}\right) - c_{N+3} \sin\left(2\pi \cdot \frac{\theta}{\eta_N/2^3}\right)$$

$$\cdots \quad (9)$$

TABLE I
ERROR COEFFICIENTS

N values	Included angle of lines η_N	Coefficient c_N
$N = 6$	$\eta_N = 2\pi/2^6$	$c_N = -6.3009''$
$N = 7$	$\eta_N = 2\pi/2^7$	$c_N = -0.7870''$
$N = 8$	$\eta_N = 2\pi/2^8$	$c_N = -0.0984''$
$N = 9$	$\eta_N = 2\pi/2^9$	$c_N = -0.0123''$
$N = 10$	$\eta_N = 2\pi/2^{10}$	$c_N = -0.0015''$
$N = 11$	$\eta_N = 2\pi/2^{11}$	$c_N = -0.0002''$

In application, the θ/η_N value can then be computed.

$$\frac{\theta}{\eta_N} = \frac{x_b}{x_b - x_a}. \quad (10)$$

Incorporating (10) into (9) enables the compensation for the measurement error caused by the low-density code disk.

IV. SIMULATION

A. Simulation of Model Coefficients

To accurately obtain the harmonic coefficient c_N, the least-squares method was used to fit the error values in (8). It can be seen from (8) that when $N = 5$, the model in (8) includes all harmonic error components when $N = 6$, $N = 7$, $N = 8$, $N = 9$, $N = 10$, $N = 11$, etc. Therefore, in order to obtain the coefficient c_N when $N = \{11, 10, 9, 8, 7, 6\}$, $N = 5$ can be set directly. All model parameters can be obtained by fitting the harmonic model when $N = 5$. The harmonic error model (8) when $N = 5$ is fitted. The fitted objective function is shown in (7).

By fitting, the c_N coefficients obtained are shown in Table I. In the error compensation operation, the coefficients in Table I will be directly used to achieve error compensation.

B. Simulation of Model Parameters

To verify the accuracy of the harmonic error compensation algorithm in (8), MATLAB software was used to simulate the system. When $N > 8$, the amplitude of the error curve is very small, so only simulations for the cases where $N \leq 8$ were included in the verification.

The data in Table I were substituted into (8) to calculate the difference between the harmonic error model (8) and the real model (7). The comparison curve between the error model and harmonic model is shown in Fig. 6(a); the difference curves obtained through simulations are shown in Fig. 6(b).

The error caused by the low-density code disk can be significantly reduced by applying the proposed harmonic error model. When $N = 6$, the differences between the harmonic error model and the actual error model are less than $\pm 0.3''$. When $N = 7$, the differences are less than $\pm 0.05''$, and when $N = 8$, the differences are almost zero.

Therefore, it can be concluded that the error compensation algorithm based on the harmonic model in (8) can effectively reduce the error induced by a low-density code disk.
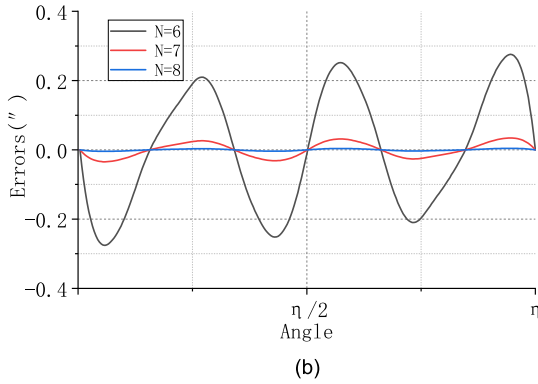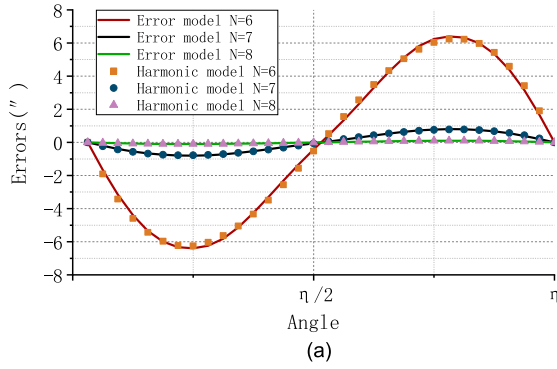
Fig. 6.   Comparison curves. (a) Comparison curve of error model and harmonic model. (b) Difference curves between the error model and harmonic model.
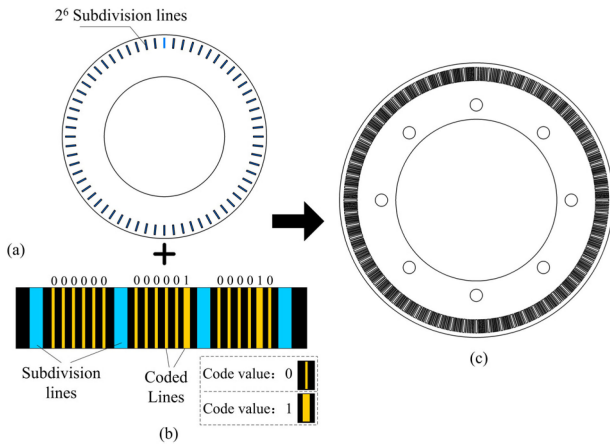

Fig. 7.   Principle of experimental coding.

V. EXPERIMENTS

To test the performance of the proposed error compensation algorithm, an experimental grating disk with a diameter of 62 mm was designed. All lines were engraved in a circle with a diameter of 57 mm, and there was a total of $2^N = 64$ lines in the circle, as shown in Fig. 7(a). To ensure successful absolute displacement measurements in the experiments, the corresponding binary codes were marked between the 64 lines to identify absolute position information. The values of the inserted binary
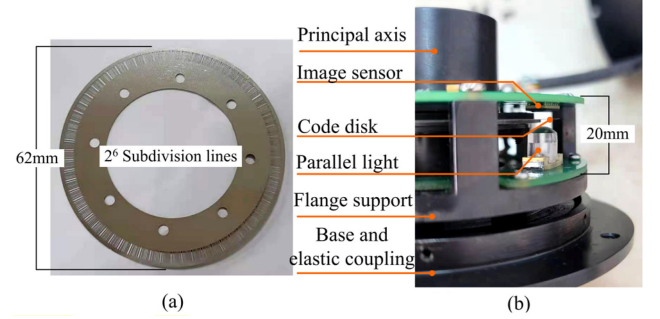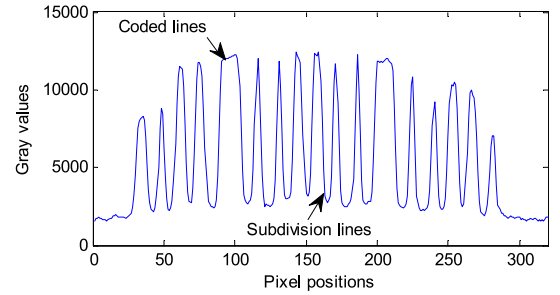

Fig. 8.   LI-ADM experimental device.

Fig. 9.   Pixel information of LI-ADM experimental device.

codes ranged between "000 000" and "111 111", as shown in Fig. 7(b).

Meanwhile, a displacement measurement device was designed based on the principle of LI-ADM and using the experimental grating disk shown in Fig. 8.

Based on the measuring device in Fig. 8, the pixel information collected by the linear scan image sensor is shown in Fig. 9. It can be seen that the lines with wide pixel range in the figure are "coded lines" and the lines with narrow image are "subdivision lines."

According to this experimental grating disk, when using the measurement algorithm in (1), the subdivision multiple can be defined as $2^M = 2^{17}$. Therefore, with $2^N = 2^6 = 64$ lines in the upper circle, an overall $M+N = 17+6 = 23$-b LI-ADM resolution can be achieved.

When we design the LI-ADM measuring device, "installation error of shafting" must be controlled to the minimum. At the same time, to eliminate the error caused by "shafting error" and other factors when installing the grating code disk, the two image sensors are respectively placed at the opposite diameter position of the circular grating. The "installation" error is eliminated through the average value of the measured data of two image sensors. In the experiment of this article, the factors such as "installation error" of grating code disk have been eliminated by the dual image sensor.

A. Accuracy Test Before Error Compensation

To verify the accuracy of this LI-ADM system, a 17-polyhedron and laser autocollimator were used for error detection with the experimental device, as shown in Fig. 10.
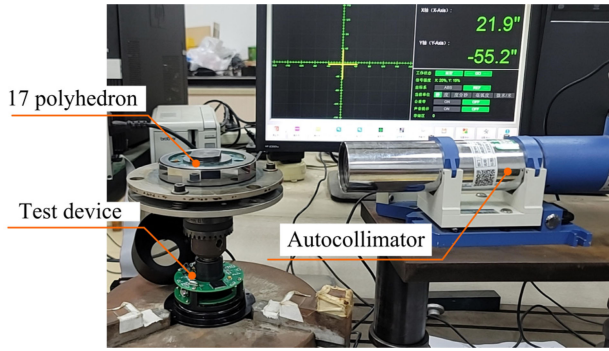
Fig. 10. Error testing equipment.

Fig. 11. Comparison of errors before and after compensation.

TABLE II
ERROR WHEN USING THE PROPOSED GRATING DISK

No.	Error (")	No.	Error (")
1	0	10	−2.5
2	−8.5	11	16.5
3	7.4	12	15.6
4	16.6	13	19.8
5	13.9	14	3.9
6	1.7	15	0.7
7	13.1	16	11.4
8	16.8	17	10.6
9	5.3		

TABLE III
ERROR WHEN USING N = 9 GRATING DISK

No.	Error (")	No.	Error (")
1	0	10	−0.8
2	−1.6	11	12.5
3	5.2	12	6.5
4	8.9	13	10.8
5	8.3	14	2.4
6	5.9	15	4.2
7	12.5	16	8.7
8	11.2	17	4.4
9	−1.2		

During the experiment, the 17-polyhedron was coaxially connected to the experimental device, and then the error value was collected by the autocollimator; up to 17 positions of error data could be obtained. The results of these error tests are presented in Table II, and the mean squared error of the values in Table II is $\sigma_1 = 8.14''$.

B. Error Compensation Test

The error compensation algorithm proposed in (8) was applied to the experimental testing device. Again, 17-polyhedrons were considered for the error testing, and the obtained results are presented in Table III. The mean squared error of the values in Table III is $\sigma_2 = 4.78''$.

A comparison of the error curves before and after compensation is shown in Fig. 11. It can be seen that the variation range of error is reduced from $\{-8.5 \sim 19.8\}$ to $\{-1.6 \sim 12.5\}$.
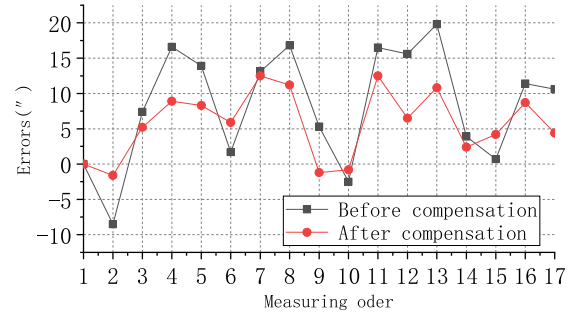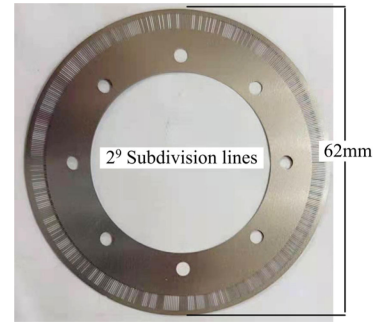

Fig. 12. Grating disk with $2^N = 2^9$ used for comparison.

The standard deviation of error is reduced from 8.14 "to 4.78". After applying the proposed error compensation algorithm, the fluctuation range of the error curve was significantly reduced, and the error compensation algorithm was deemed effective for practical applications.

C. Accuracy Comparison Experiment

According to the error curve in Fig. 4, when a grating disk with $N = 9$ was used, the measurement error based on the linear image was almost zero. For this reason, the grating disks with $2^N = 2^9$ lines and $2^N = 2^6$ lines were considered when comparing the measurement errors. The grating disk designed with $2^N = 2^9$ lines is shown in Fig. 12.

The 62 mm diameter grating disk in Fig. 12 has $2^N = 512$ evenly distributed lines around the disk. After the accuracy test, the error data obtained using the $2^N = 2^9$ grating disk is shown as the red curve in Fig. 13. For comparison, the error curve of the $2^N = 2^6$ grating disk after compensation is also plotted in Fig. 13 (black curve).

The computational accuracy achieved when using an $N = 9$ grating disk was $\sigma_{N=9} = 4.19''$, and the measurement accuracy using an $N = 6$ grating disk after error compensation was $\sigma_{N=6} = 4.78''$. These comparative results demonstrate that the accuracy achieved by the two measurement methods were similar. Therefore, although the line density of the $N = 6$ grating disk was relatively low, the error caused by the low-density lines can be reduced following an appropriate error compensation.
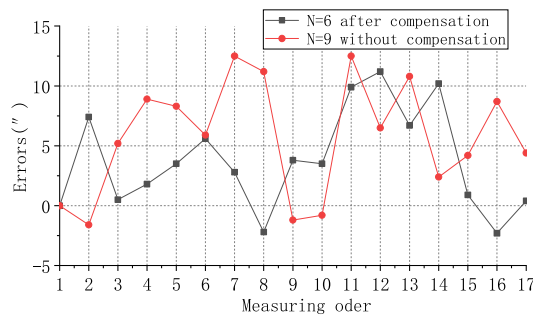
Fig. 13.   Error curve comparison.

VI. CONCLUSION

LI-ADM technology based on a single-track code disk could achieve higher robustness and fault tolerance than traditional photoelectric displacement measurement technology. According to previous research, when designing a small-size LI-ADM device, the diameter of the circular grating used was also relatively small. Due to the limited pixel size, the circular grating could not place more lines when realized single channel absolute coding recognition on a small diameter grating disk. However, in the LI-ADM algorithm, lower-density lines lead to measurement errors. Therefore, this article proposed an error compensation method for low-density code disks.

First, the principle of LI-ADM technology and the displacement measurement algorithm based on image recognition were explained. Second, the measurement error caused by the low-density grating disk was analyzed, and an error model was established. Then, according to the established error model, an error compensation algorithm was proposed. Finally, simulation and experimental verifications confirmed that the proposed error compensation algorithm could significantly reduce the measurement error caused by the low-density marking coded disk. The results presented herein provide a theoretical foundation for improving the accuracy of image-type displacement measurement technologies.

Of course, for the harmonic error in displacement measurement, the error compensation method proposed in this article was not the only one. In the follow-up research, we would continue to study the method of removing harmonic error by using multiple linear scan image sensors, so as to realize higher precision displacement measurement.

REFERENCES

[1] Z. Chen, X. Liu, K. Peng, Z. Yu, and H. Pu, "A self-adaptive interpolation method for sinusoidal sensors," *IEEE Trans. Instrum. Meas.*, vol. 69, no. 10, pp. 7675–7682, Oct. 2020.
[2] Z. Chen and M. Segev, "Highlighting photonics: Looking into the next decade," *eLight*, vol. 1, 2021, Art. no. 2.
[3] Y. Lu and W. Hu, "Angular measurement of high precision reducer for industrial robot," *IEEE Trans. Instrum. Meas.*, vol. 70, 2021, Art. no. 1002410.
[4] K. Hane, T. Endo, M. Ishimori, and M. Sasaki, Sens, "Integration of grating-image-type encoder using si micromachining," *Actuators A*, vol. 97, pp. 139–146, 2002.
[5] Z. Yu, K. Peng, X. Liu, Z. Chen, and Y. Huang, "A high-precision absolute angular-displacement capacitive sensor using three-stage time-grating in conjunction with a remodulation scheme," *IEEE Trans. Ind. Electron.*, vol. 66, no. 9, pp. 7376–7385, Sep. 2019.
[6] N. Anandan and B. George, "A wide-range capacitive sensor for linear and angular displacement measurement," *IEEE Trans. Ind. Electron.*, vol. 64, no. 7, pp. 5728–5737, Jul. 2017.
[7] Z. Zhang *et al.*, "A novel absolute angular position sensor based on electromagnetism," *Sensors Actuators A*, vol. 194, pp. 196–203, 2013.
[8] Z. Chen, H. Pu, X. Liu, D. Peng, and Z. Yu, "A time-grating sensor for displacement measurement with long range and nanometer accuracy," *IEEE Trans. Instrum. Meas.*, vol. 64, no. 11, pp. 3105–3115, Nov. 2015.
[9] H. Yu, J. X, W. Q, L. Liang, and C. Zhao, "High-resolution angular displacement technology based on varying moiré figure phase positions," *IEEE Sensors J.*, vol. 19, no. 6, pp. 2126–2132, Mar. 2019.
[10] H. Yu, Q. Wan, Y. Sun, X. Lu, and C. Zhao, "High precision angular measurement via dual imaging detectors," *IEEE Sensors J.*, vol. 19, no. 17, pp. 7308–7312, Sep. 2019.
[11] J. Xu *et al.*, "Virtual moiré fringe for grating measurement system based on CMOS microscopic imaging," *Proc. SPIE*, vol. 785325, pp. 1–5, 2010.
[12] S. Das and T. S. Sarkar, "A new method of linear displacement measurement utilizing grayscale image," *Int. J. Electron. Elect. Eng.*, vol. 1, no. 3, pp. 176–181, 2013.
[13] H. Yu, Q. Wan, C. Zhao, C. Zhao, and Y. Sun, "Anti-stain algorithm of angular displacement based on a single image sensor," *Appl. Opt.*, vol. 59, no. 7, pp. 1985–1990, 2020.
[14] D. B. Leviton and B. J. Frey, "Ultra-high resolution, absolute position sensors for cryostatic applications," *Proc. SPIE*, vol. 4850, pp. 776–787, 2003.
[15] Y. Sugiyam *et al.*, "A 3.2 kHz 14-bit optical absolute rotary encoder with a CMOS profile sensor," *IEEE Sensors J.*, vol. 8, no. 8, pp. 1430–1436, Aug. 2008.
[16] J. S. Baji, D. Z. Stupara, and B. M. Dakib, "An absolute rotary position sensor based on cylindrical coordinate color space transformation," *Sensors Actuators A. Phys.*, vol. 213, pp. 27–34, 2014.
[17] J. A. Kim *et al.*, "Absolute angle measurement using a phase-encoded binary graduated disk," *Measurement*, vol. 80, pp. 288–293, 2016.
[18] Y. Mu *et al.*, "A 7.4 kHz, 20 bit image encoder with a CMOS linear image sensor," *Opt. Quantum Electron.*, vol. 51, 2019, Art. no. 321.
[19] P. Yuan *et al.*, "An anti-spot, high-precision subdivision algorithm for linear CCD based single-track absolute encoder," *Measurement*, vol. 137, pp. 143–154, 2019.
[20] H. Yu, Q. Wan, Y. Sun, X. Lu, and C. Zhao, "High precision angular measurement via dual imaging detectors," *IEEE Sensors J.*, vol. 19, no. 17, pp. 7308–7312, Sep. 2019.
[21] H. Yu, Q. Wan, X. Lu, Y. Du, and C. Zhao, "Error-correct arithmetic for angular displacement measurement when using single linear image detector," *Opt. Eng.*, vol. 57, no. 5, 2018, Art. no. 054108.
[22] H. Yu *et al.*, "Small-size, high-resolution angular displacement measurement technology based on an imaging detector," *Appl. Opt.*, vol. 56, no. 3, pp. 755–760, 2017.
[23] H. Yu, Q. Wan, Z. Mu, Y. Du, and L. Liang, "Novel nano-scale absolute linear displacement measurement based on grating projection imaging," *Measurement*, vol. 182, 2021, Art. no. 109738.

Hai Yu was born in Jilin province, China, in 1987. He received the B.S. degree in electronic information science and technology from Northeast Dianli University, Jilin, China, in 2009 and received the Ph.D. degree in mechanical and electronic engineering from the University of Chinese Academy of Sciences, Beijing, China, in 2014.

Since 2017, he has been a Project Leader for several Natural Science Foundation of China and other agency-funded projects. He was funded by the "Dawn" talent training program of Changchun Institute of Optics, Fine Mechanics and Physics, Chinese Academy of Sciences (CIOMP), in 2020. He is currently an Associate Researcher with the R&D Center for Precision Instruments and Equipment, CIOMP. His research interest includes electro-optical displacement precision measurement

Qiuhua Wan was born in Jilin province, China, in 1962. She received the Ph.D. in optical engineering from the University of Chinese Academy of Sciences, Beijing, China, in 2009.

She is currently a Researcher with the R&D Center for Precision Instruments and Equipment, CIOMP. Her research interest includes electro-optical displacement precision measurement.

Qingyang Han was born in Heilongjiang province, China, in 1988. He received the master's degree in instrument science and technology from the Beijing University of Aeronautics and Astronautics, Beijing, China, in 2013.

He is currently an Assistant Researcher of CIOMP. His research interest includes photoelectric angular displacement measurement and signal processing.

Changhai Zhao was born in Henan province, China, in 1980. He received the Ph.D. degree in mechanical and electronic engineering from the University of Chinese Academy of Sciences, Beijing, China, in 2008.

He is currently an Associate Researcher with the R&D Center for Precision Instruments and Equipment, CIOMP, Changchun, China. His research interest includes electro-optical displacement precision measurement.

Zhiya Mu was born in Shanxi province, China, in 1985. He received the Ph.D. degree in mechanical and electronic engineering from the University of Chinese Academy of Sciences, Beijing, China, in 2014.

He is currently an Associate Researcher with the R&D Center for Precision Instruments and Equipment, CIOMP. His research interest includes camera imaging technology and signal processing technology.